Jurnal Penelitian Fisika dan Aplikasinya (JPFA)
Volume 13, Issue 01, June 2023
https://journal.unesa.ac.id/index.php/jpfa/

p-ISSN: 2087-9946
e-ISSN: 2477-1775

Structural and Optical Properties of Bismuth-doped Cerium Oxide Prepared at a Low Temperature

Safira Arta Paramita [a], Iis Nurhasanah [b,*], and Ali Khumaeni [c]

Department of Physics, Faculty of Science and Mathematics, Universitas Diponegoro
Jalan Prof Soedarto, Semarang 50275, Indonesia

e-mail: [a] safiraartap@students.undip.ac.id, [b] nurhasanah@fisika.fsm.undip.ac.id, and [c] khumaeni@fisika.fsm.undip.ac.id
* Corresponding Author

Received: 8 February 2023; Revised: 20 May 2023; Accepted: 29 May 2023

Abstract

Cerium oxide (CeO_2) is a functional material with excellent physicochemical properties. Its properties can be modified by doping with different elements, including bismuth, which can be done through various synthesis methods. The precipitation method combined with ultrasonic radiation was used to synthesize bismuth-doped cerium oxide (CeO_2:Bi) at a low temperature of 200°C. In this study, we investigate the alteration of structural and optical properties of as-prepared CeO_2:Bi by subjecting it to additional calcination at a high temperature of 500°C. The structural and optical properties of CeO_2:Bi were characterized using thermal gravimetric analysis, X-ray diffraction, Scanning Electron Microscope-Energy Dispersive X-Ray, Fourier Transform Infrared spectroscopy, and UV-Visible spectroscopy. The additional calcination produced a less significant weight-loss percentage than the as-prepared CeO_2:Bi observed from the gravimetric curve. The Fourier transform infrared spectrum revealed the loss of a small number of hydroxyl molecules trapped on the CeO_2:Bi surface when additional calcination was subjected. Based on the X-ray diffraction spectra, additional calcination results in the smallest crystallite size and compressive strain without the changed cubic crystal structure of CeO_2:Bi. The successful doping of Bi in CeO_2 was confirmed by the composition analysis from Energy Dispersive X-Ray measurement. Scanning electron microscope image showed spherical and agglomerated particles of calcined CeO_2:Bi. The optical properties of both CeO_2:Bi possessed similar trend absorption spectra and almost the same band gap energy. The results indicated that the calcination of as-prepared CeO_2:Bi at a temperature of 500°C did not affect its structural and optical properties significantly. Thus, combining ultrasonic radiation with precipitation is an advantageous method to synthesize at a low temperature of stable CeO_2:Bi crystalline.

Keywords: *CeO_2; precipitation method; ultrasonic irradiation; structural properties; optical properties*

How to cite: Paramita S A, et al. Structural and Optical Properties of Bismuth-doped Cerium Oxide Prepared at Low temperature. *Jurnal Penelitian Fisika dan Aplikasinya (JPFA)*. 2023; **13**(1): 16-24.

INTRODUCTION

Cerium (Ce) is a lanthanide element largely distributed on the earth's surface, and it is one of the highest reactive rare-earth elements [1,2]. Cerium can exist in bulk form of cerium dioxide (CeO_2) and dicerium trioxide (Ce_2O_3) from valence state tetravalent (Ce^{4+}) and trivalent (Ce^{3+}) [3]. Cerium oxide with a valence of 4+ is a more stable form than 3+, as extensively studied by many scientists [4].

CeO_2 is an important functional material with low toxicity [5,6]. On the other hand, CeO_2 exhibits unique physicochemical properties such as excellent thermal and chemical stability [7,8], high absorption [4,9], and strong conductivity [10]. Due to this property, CeO_2 can be

DOI: 10.26740/jpfa.v13n1.p16-24

applied in several fields, including fuel oxidation catalysis [11,12], UV absorbers [13,14], and sunscreen [15,16]. CeO_2 has a band gap energy (E_g) between 2.6 and 3.2 eV, which depends on the synthesis method [17,18]. Many physicochemical properties of CeO_2, including the structure and thermal stability, optical absorption, electro-conductivity, and others, can be modified by doping CeO_2 with different elements. The elements used as a dopant depend on the valence and the atomic radii of the constituents [19]. One of the elements that can be used as a dopant to modify the structural and optical properties of CeO_2 is bismuth (Bi) [8,20]. Bi has a valence of 3+ and an ionic radius of 1.03 Å that is larger than an ionic radius of Ce^{4+} (0.97 Å). Generally, dopants with a larger ionic radius are difficult to replace lattice host atoms. Therefore, the synthesis procedure to produce crystalline bismuth-doped CeO_2 (CeO_2:Bi) is usually carried out at high-temperature [21]. Several methods that can be used for the synthesis of CeO_2:Bi include hydrothermal [22], sol-gel hydrothermal [23], sol-gel [24], and precipitation [21]. Due to its low calcination process, the hydrothermal method has been adopted as a preferable method. However, this process requires a long time of up to 24 hours, whereas, in the sol-gel method, the doping process is carried out through a calcining process at a high temperature in a moderate time. In contrast, precipitation is simpler because it goes through a short calcining process with a moderate temperature. To substitute Bi doping into the CeO_2 lattice and form crystalline CeO_2:Bi at a low temperature and a short time without going through a high calcining process, ultrasonic radiation is applied to precipitation [25].

This study investigates the formation of CeO_2:Bi crystalline at a low temperature and a short time using a precipitation process combined with ultrasonic radiation. The obtained CeO_2:Bi was characterized using X-ray Diffraction (XRD), Scanning Electron Microscope-Energy Dispersive X-Ray (SEM-EDX), Thermal Gravimetric Analysis (TGA), Fourier Transform Infrared Spectroscopy (FTIR), and UV-Vis analysis. The structural and optical properties of as-prepared CeO_2:Bi were compared to CeO_2:Bi calcined at 500°C.

METHOD

Preparation of CeO_2:Bi

CeO_2:Bi was synthesized using the precipitation method combined with ultrasonic radiation. Cerium Nitrate Hexahydrate ($Ce(NO_3)_3.6H_2O$) (Sigma-Aldrich, 99%) 0.08 M and 5% molar ratio of $Bi(NO)_3.5H_2O$) (Sigma-Aldrich, 99%) were used as a precursor. Both were dissolved in demineralized water and isopropanol (Merck) and then stirred until homogeneous. The precipitation process was carried out by dripping a precipitant of a 3 M ammonium solution (Merck) until it reached a pH of 10. Furthermore, the solution was irradiated by ultrasonic. The result of the precipitate was washed using distilled water and ethanol (Merck). CeO_2:Bi powder is formed after going through a drying process at 200 °C for 3 hours. In this case, the structural and optical properties of as-prepared CeO_2:Bi and the CeO_2:Bi calcined at 500 °C were characterized.

Characterizations

Phase changes and thermal stability of CeO_2:Bi powders were studied using thermogravimetric analysis (TGA) (Hitachi STA200RV) from ambient temperature until 900 °C. The crystal structure of the CeO_2:Bi was analyzed using an X-Ray diffractometer (XRD) (Rigaku MiniFlex). The Williamson-Hall equation (1) was applied to obtain the crystallite size (D) and lattice strain of the CeO_2:Bi.

$$\beta \cos \theta = \frac{K}{D} + 4\varepsilon \sin \theta \quad (1)$$

where θ, β, D, ε, and K are diffraction angle, FWHM, crystallite size, lattice strain, and a constant of 0.94 respectively. Equation (2) was used to determine lattice parameter (a),

$$a = \frac{\sqrt{h^2 + k^2 + l^2}}{2\ sin\ \theta} \tag{2}$$

where h, k, l is the Miller index.

Scanning Electron Microscope-Energy Dispersive X-Ray (SEM-EDX) (JEOL JSM-6510LA) was used to analyze the morphology and elemental composition of the CeO_2:Bi. The functional groups and chemical bonds were identified using Fourier transform infrared spectroscopy (FTIR) (PerkinElmer Spotlight 200i). The optical properties were examined using UV-Visible spectroscopy (Shimadzu). The Tauc plot method was utilized to estimate the band gap energy (E_g) by extrapolating the straight line of the curves of equation (3).

$$(\alpha hv)^2 = C\left(hv - E_g\right) \tag{3}$$

where h is the Planck constant, v is photon frequency, C is a constant, E_g is the band gap energy, and α is the absorption coefficient.

RESULTS AND DISCUSSION

Thermal Gravimetric Analysis

Thermal gravimetric analysis (TGA) measurement was applied to examine the thermal stability of as-prepared and calcined CeO_2:Bi. TGA is usually a good technique for testing manufactured materials' thermal and structural stability [7]. This study experimentally used temperatures in the range of 23-900 °C. As shown in Figure 1, the thermogram curves of the as-prepared CeO_2:Bi shows two steps of weight loss: the first involves 3.42 wt% starting at 23-120°C due to water evaporation, and the second involves 3.51 wt% due to the removal of a few of hydroxyl molecules at 120 – 480 °C, which is remain attached on the Ce atoms. This means that crystallization of the CeO_2:Bi molecule is more established at this step, and after 480 °C, the sample is more stable. This slight decrease in total weight loss indicates that the as-prepared sample has formed CeO_2 in a stable phase. Meanwhile, the calcined CeO_2:Bi just shows one weight-loss stage, which occurs at a temperature of 23-120 °C, equivalent to removing H_2O molecules [12,26]. The hydroxyl molecules were lost in the calcined CeO_2:Bi sample, so there was no weight loss step after 120 °C. That means the CeO_2:Bi is stable above 120°C without phase change. The calcination at a high temperature of 500°C only causes the loss of a few hydroxyl molecules bound in CeO_2:Bi. Further, the weight loss only correlated with the trapped water evaporation; thus, the CeO_2:Bi becomes more stable.

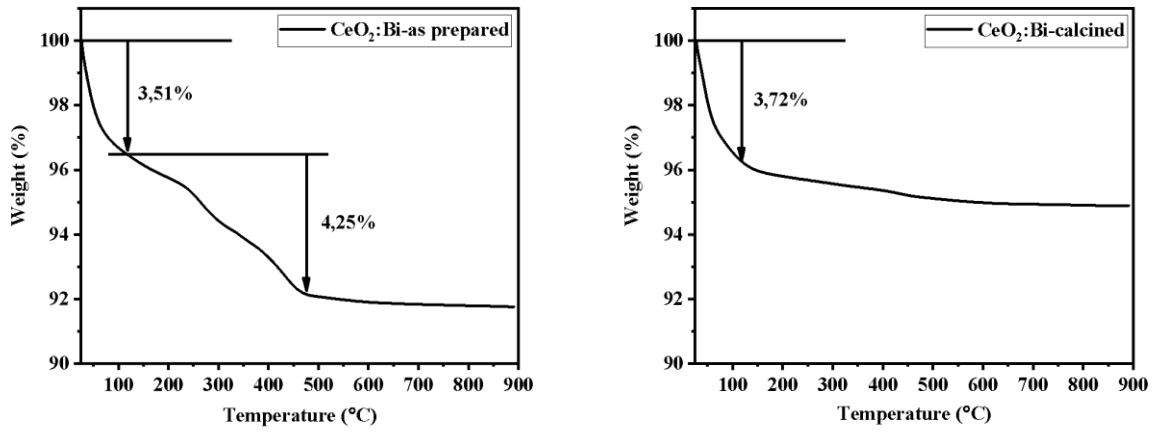

Figure 1. TGA Curves of (a) CeO_2:Bi-as Prepared and (b) CeO_2:Bi-Calcined

Structure Analysis

FTIR Analysis

Figure 2 shows the FTIR spectrum of CeO_2:Bi for identifying the surface chemical bonds and their functional groups. The O-H stretching vibration is thought to cause the wide broadband at 3566 cm^{-1} for CeO_2:Bi-as prepared and at 3443 cm^{-1} for CeO_2:Bi-calcined [27]. The two absorption bands at 2368 cm^{-1} and 1832 cm^{-1} (CeO_2:Bi-as prepared), 2353 cm^{-1} and 1537 cm^{-1} (CeO_2:Bi-calcined), indicating CO_2 trapped in the environment [28]. The strong band on CeO_2:Bi-as prepared with wavenumber 1384 cm^{-1}, leads to the hydroxyl groups trapped on the CeO_2. After calcination, the strong peaks of the hydroxyl groups in that wavenumber disappeared, resulting in a stronger Ce-O vibration peak [26]. The Ce-O stretching vibration corresponds to the strong bands at 477 cm^{-1} and 484 cm^{-1} for CeO_2:Bi-as prepared and CeO_2:Bi-calcined respectively [24,25]. This is consistent with the TGA analysis that calcination of CeO_2:Bi at a temperature of 500°C is only a weight loss due to water evaporation.

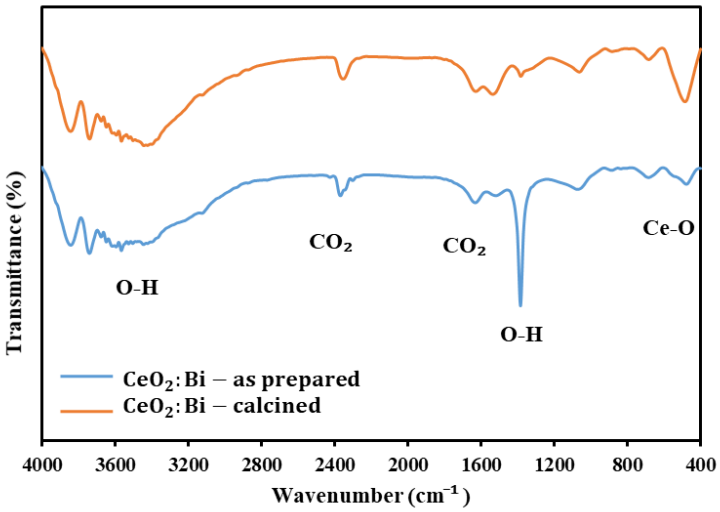

Figure 2. FTIR Spectra of CeO_2:Bi-as Prepared and CeO_2:Bi-Calcined

XRD Analysis

Structural characteristics of both CeO_2:Bi were analyzed using XRD measurements. The intensity of the diffracted beam as a function of the diffraction angle showed in Figure 3. The as-prepared and calcined CeO_2:Bi diffraction peaks were attributed to the face-centered cubic fluorite CeO_2 (JCPDS 34-0394 and COD 497333). In general, the addition of doping will shift the diffraction peaks resulting in an increase or decrease in the lattice parameter. The lattice parameters calculated for both CeO_2:Bi using Equation (2) are 5.4109 Å and 5.4299 Å for as-prepared and calcined. This result agrees with the reference's lattice parameter (JCPDS 34-0394 and COD 497333) and previous studies [21,23,24]. The diffraction peak of the calcined CeO_2:Bi shifted to the left of 2θ, resulting in a larger lattice constant than as prepared CeO_2:Bi. The addition of calcination results in a decreased intensity and shifted x-ray diffraction peaks. The possible mechanism explanation is the restructuring of the surface atoms due to the release of hydroxyl [29]. The non-appearance of a secondary phase in the XRD pattern of CeO_2:Bi indicates that CeO_2 has been formed with the fluorite structure maintained despite the Bi dopant's addition.

As is commonly known, high crystallinity of CeO_2 can be achieved through calcination at high a temperature for a prolonged period, as demonstrated in a study by Hebert et al, where they used a temperature of 800°C for 5 hours [21]. In this study, CeO_2:Bi exhibited high crystallinity with a low heating process due to the addition of ultrasonic radiation [25].

Ultrasonic radiation induces a chemical effect through acoustic cavitation, which involves the formation, growth, and collapse of bubbles in a liquid medium, leading to instantaneous high temperature and pressure [30,31]. Thus, it can be concluded that ultrasonic radiation can accelerate the formation of CeO_2:Bi crystals and reduced the calcination temperature. The application of ultrasonic radiation on the synthesis of CeO_2:Bi demonstrates that the continued heating process did not alter the structural characteristic of CeO_2.

The addition of calcination to CeO_2:Bi results in a shift in the diffraction peaks and a lattice parameter, which correlated to crystallite size and micro-strain. Figure 4 depicts the Williamson-Hall plot, which is used to clarify the crystallite size and micro-strain of both CeO_2:Bi. By taking the slope of the linear fitting of the data, the micro-strain for the prepared CeO_2:Bi shows a positive value of 0.0049, which indicates that the sample is experiencing tensile strain. Meanwhile, for the calcined CeO_2:Bi, the micro-strain shows a negative value of 0.0056, indicating compressive strain. This shows that the addition of calcination causes a decreasing trend of lattice strain. This value corresponds to a decreasing crystallite size of calcined CeO_2:Bi. The as-prepared and calcined CeO_2:Bi had crystallite sizes of 9.85 nm and 4.81 nm, respectively, obtained from the intercept of Williamson-Hall plots (Figure 4).

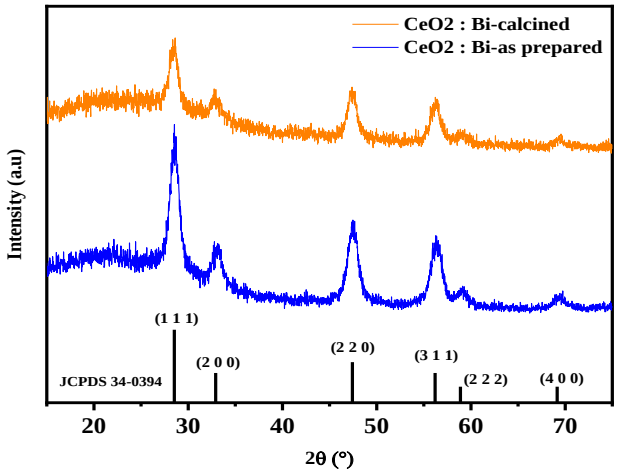

Figure 3. XRD Patterns of CeO_2:Bi-as Prepared and CeO_2:Bi-calcined

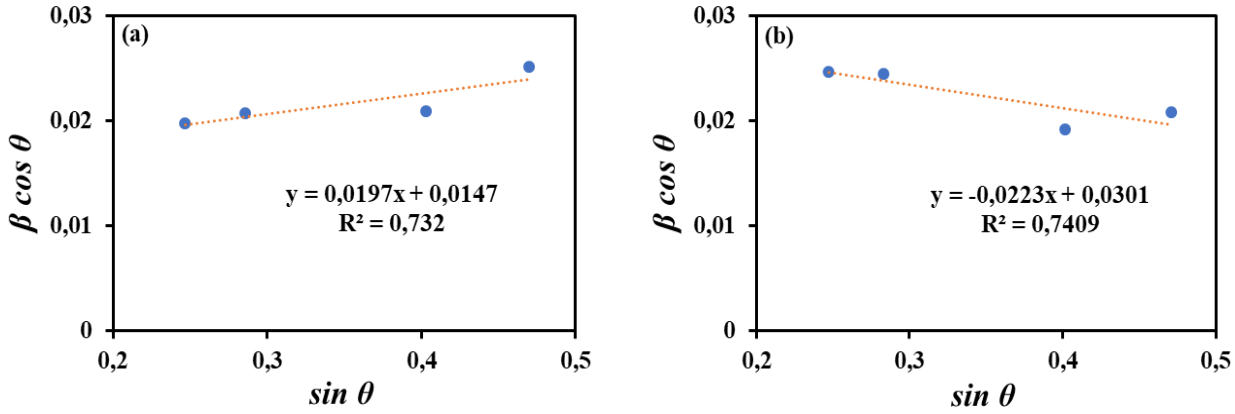

Figure 4. Williamson–Hall Plots of (a) CeO_2:Bi-as Prepared and (b) CeO_2:Bi-calcined

Microscopy Analysis

To investigate the morphology, the samples were scanned under an SEM microscope. SEM images for (a) CeO_2:Bi-as prepared and (b) CeO_2:Bi-calcined is shown in Figure 5. The SEM image of the as-prepared CeO_2:Bi displayed particles with better uniformity in size, while the

SEM image of CeO_2:Bi treated with calcination showed particles with greater agglomeration. The calcination treatment at a temperature of 500°C induced the coalescence of particles, producing agglomerated particles.

The presence of Bi as a dopant in CeO_2 was confirmed by analyzing the mass percentages of Ce, O, and Bi atoms using EDX. As inserted in Figure 5, Ce, O, and Bi mass percentages in the as-prepared CeO_2:Bi were 77.94%, 18.24%, and 3.82%, respectively. On the other hand, Ce, O, and Bi mass percentages in the calcined-CeO_2:Bi were 87.09%, 6.24%, and 6.67%, respectively. The mass percentage of Bi atoms in both as-prepared and calcined-CeO_2:Bi confirms the inclusion of Bi into CeO_2. Based on the stoichiometric composition of Ce and O in CeO_2 i.e., Ce (81.39%) and O (18.61%), the as-prepared CeO_2:Bi shows that Ce and O mass percentage are lower and close to the stoichiometric value. The result can be attributed to the incorporation of Bi^{3+} dopant into the Ce^{4+} lattice led to an imbalance in the distribution of electric charges and the presence of oxygen vacancy in CeO_2 [21–23]. In addition, the Bi mass percentage of 3.82% corresponds to calculating the molar ratio of Bi precursor. Meanwhile, the mass percentage of Ce and O in calcined-CeO_2:Bi show alteration from the stoichiometric composition. The introduction of calcination in as-prepared CeO_2:Bi leads to hydroxyl evaporation. Consequently, it reduces the O mass percentage. The EDX analysis indicated that the ultrasonic irradiation and heating process at a temperature of 200°C successfully formed CeO_2:Bi crystalline with cubic fluorite of CeO_2, in agreement with the XRD results as shown in Figure 3.

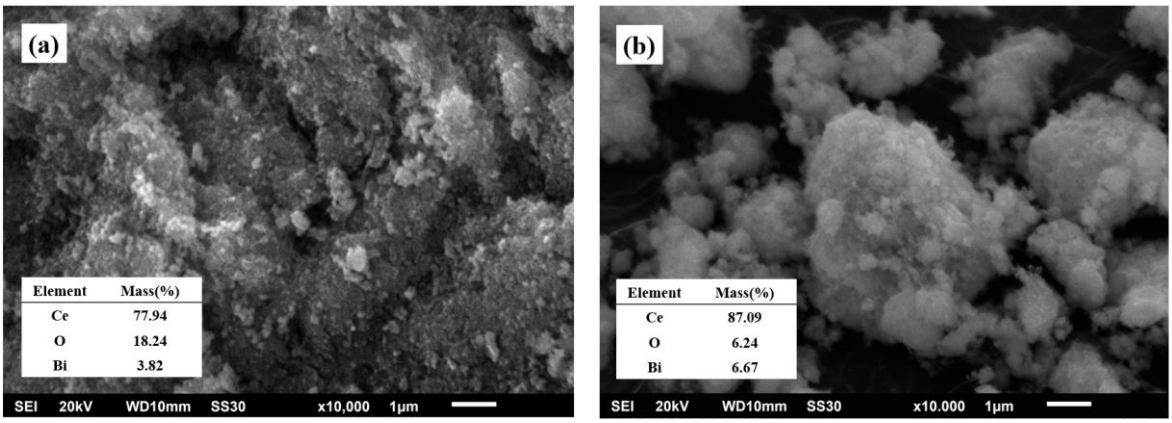

Figure 5. SEM Images of (a) CeO_2:Bi-as Prepared and (b) CeO_2:Bi-calcined

UV–VIS Analysis

Figures 6 (a) and 6 (b) show the optical absorption spectrum and band gap plots of both CeO_2:Bi. Generally, high absorption in the 200–400 nm visible region is present in all CeO_2:Bi samples. The intersection of the x-axis with the linear segment of the Tauc plot curve determines the value of E_g. The results in Figure 6 (b) demonstrated a slight shift in E_g from 3.02 to 2.99 eV for CeO_2:Bi as-prepared and calcined. According to other reports, a decrease in the bandgap energy is attributed to the reduction in oxygen due to the calcination process, resulting in a higher concentration of oxygen vacancies compared to CeO_2:Bi-as prepared [23,24]. The UV absorbance spectrum profile of CeO_2:Bi shows excellent optical properties with no significant differences observed between the as-prepared and calcined samples. However, the addition of calcination slightly reduces the absorbance and the absorption end, which can be seen from the energy band gap.

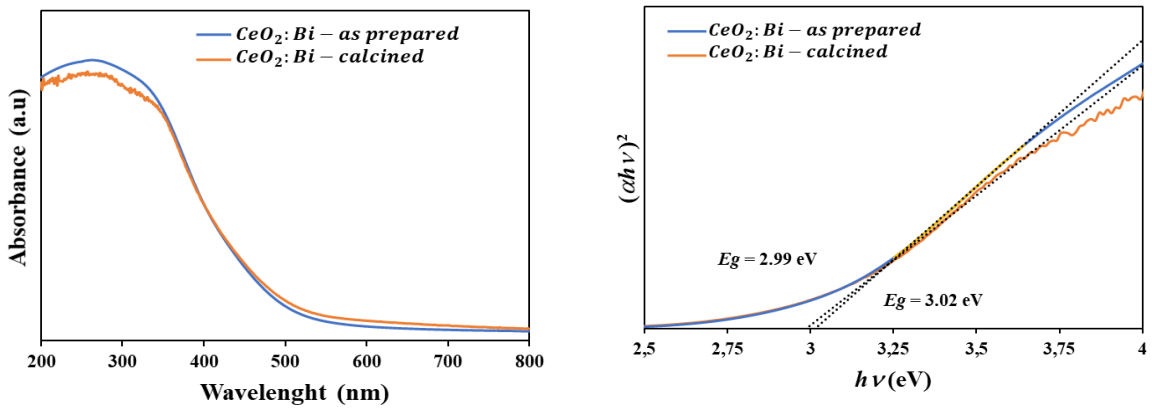

Figure 6. (a) Optical Absorption Spectrum and (b) Band Gap Plots of CeO_2:Bi-as Prepared and CeO_2:Bi-Calcined

Despite the hopeful results, certain limitations to our study must be addressed. This work only examined the CeO_2 structural and optical properties under controlled conditions. The findings may differ depending on the synthesis circumstances. More research is needed to explore the structural and optical properties of CeO_2 with varying Bi concentrations. Furthermore, future research should investigate how varied preparation circumstances, such as pH and reaction time, affect the characteristics of CeO_2:Bi.

This discovery substantially impacts the field of physics since it provides essential insights into the properties of Bi-doped CeO_2 and its potential applications, including optics, catalysis, and energy conversion. Investigating the structural and optical properties of CeO_2:Bi gives a better understanding of its properties and prospective applications.

CONCLUSION

CeO_2:Bi has been successfully synthesized using a precipitation method combined with ultrasonic radiation. The TGA curve displays one-step weight loss in the calcined CeO_2:Bi compared to the as-prepared CeO_2:Bi. The weight loss is attributed to a slight loss of hydroxyl molecules trapped on the surface of CeO_2:Bi and produces a sharper Ce-O group. The addition of calcination reduces crystallite size and band gap energy but does not change the phase structure of CeO_2. The successful incorporation of Bi into CeO_2, as verified through XRD analysis, is additionally reinforced by the findings derived from EDX measurements. According to the SEM image, the morphology of CeO_2:Bi calcined formed spherical and agglomerate particles. The results showed that the precipitation method combined with ultrasonic radiation produced the stable CeO_2:Bi crystalline at a low temperature. Furthermore, the development of a new synthesis method that is faster and more efficient can accelerate the production of CeO_2:Bi and thus has the potential to be applied in various fields.

AUTHOR CONTRIBUTIONS

Safira Arta Paramita: Investigation, data collection, analysis, and writing of original draft; Iis Nurhasanah: Conceptualization, supervising, validation, analysis, and writing; and Ali Khumaeni: reviewing and editing the final manuscript.

DECLARATION OF COMPETING INTEREST

The authors declare that they have no known competing financial interests or personal relationships that could have appeared to influence the work reported in this paper.

REFERENCES

[1] Zhang J, Liu Q, He Q, and Nozaki Y. Rare Earth Elements and Their Isotopes in the Ocean. In *Encyclopedia of Ocean Sciences*. Netherlands: Elsevier; 2019: 181–197. DOI: https://doi.org/10.1016/B978-0-12-409548-9.10855-3.

[2] Spiridigliozzi L. *Doped-Ceria Electrolytes Synthesis, Sintering and Characterization*. Switzerland: Springer Cham; 2018. DOI: https://doi.org/10.1007/978-3-319-99395-9.

[3] Ranasinghe KS, et al. Evidence of the Coexistence of Multivalence Cerium Oxide Nano-Particles in a Sodium Borate Glass. *Journal of Non-Crystalline Solids*. 2019; **515**: 75–81. DOI: https://doi.org/10.1016/j.jnoncrysol.2019.04.001.

[4] Li J, et al. Distribution and Valence State of Ru Species on CeO_2 Supports: Support Shape Effect and Its Influence on CO Oxidation. *ACS Catalysis*. 2019; **9**(12): 11088–11103. DOI: https://doi.org/10.1021/acscatal.9b03113.

[5] Pujar MS, Hunagund SM, Desai VR, Patil S, and Sidarai AH. One-Step Synthesis and Characterizations of Cerium Oxide Nanoparticles in an Ambient Temperature via Co-Precipitation Method. *AIP Conference Proceedings*, 2018; **1942**: 050026. DOI: https://doi.org/10.1063/1.5028657.

[6] Garzón-Manjón A, et al. Simple Synthesis of Biocompatible Stable CeO_2 Nanoparticles as Antioxidant Agents. *Bioconjugate Chemistry*. 2018; **29**(7): 2325–2331. DOI: https://doi.org/10.1021/acs.bioconjchem.8b00300.

[7] Wang F, et al. Effect of Cerium Oxide on Phase Composition, Structure, Thermal Stability and Aqueous Durability of Sodium-Iron-Boron-Phosphate Based Glasses. *Journal of Nuclear Materials*. 2021; **556**: 153199. DOI: https://doi.org/10.1016/j.jnucmat.2021.153199.

[8] Jose S, et al. Low Temperature Synthesis of NIR Reflecting Bismuth Doped Cerium Oxide Yellow Nano-Pigments. *Materials Letters*. 2018; **233**: 82–85. DOI: https://doi.org/10.1016/j.matlet.2018.08.136.

[9] Mauro M, et al. Cerium Oxide Nanoparticles Absorption through Intact and Damaged Human Skin. *Molecules*. 2019; **24**(20): 3759. DOI: https://doi.org/10.3390/molecules24203759.

[10] Sun X, et al. Surface Protonic Conductivity in Chemisorbed Water in Porous Nanoscopic CeO_2. *Applied Surface Science*. 2023; **611**(A): 155590. DOI: https://doi.org/10.1016/j.apsusc.2022.155590.

[11] Corro G, et al. Biodiesel and Fossil-Fuel Diesel Soot Oxidation Activities of Ag/CeO_2 Catalyst. *Fuel*. 2019; **250**: 17–26. DOI: https://doi.org/10.1016/j.fuel.2019.03.043.

[12] Pal P, et al. CeO_2 Nanowires with High Aspect Ratio and Excellent Catalytic Activity for Selective Oxidation of Styrene by Molecular Oxygen. *RSC Advances*. 2013; **3**(27): 10837–10847. DOI: https://doi.org/10.1039/c3ra23485a.

[13] An K, et al. Synergistic Reinforcement Coating with Anti-Corrosion and UV Aging Resistance by Filling Modified CeO_2 Nanoflakes. *Colloids and Surfaces A: Physicochemical and Engineering Aspects*. 2021; **625**: 126904. DOI: https://doi.org/10.1016/j.colsurfa.2021.126904.

[14] Iqbal A, et al. Biogenic Synthesis of CeO_2 Nanoparticles and Its Potential Application as an Efficient Photocatalyst for the Degradation of Toxic Amido Black Dye. *Environmental Nanotechnology, Monitoring and Management*. 2021; **16**: 100505. DOI: https://doi.org/10.1016/j.enmm.2021.100505.

[15] Parwaiz S, Khan MM, and Pradhan D. CeO_2-Based Nanocomposites: An Advanced Alternative to TiO_2 and ZnO in Sunscreens. *Materials Express*. 2019; **9**(3): 185–202. DOI: https://doi.org/10.1166/mex.2019.1495.

[16] Ditlopo N, et al. From Khoi-San Indigenous Knowledge to Bioengineered CeO_2 Nanocrystals to Exceptional UV-Blocking Green Nanocosmetics. *Scientific Reports*. 2022; **12**(1): 3468. DOI: https://doi.org/10.1038/s41598-022-06828-x.

[17] Kusmierek E. A CeO_2 Semiconductor as a Photocatalytic and Photoelectrocatalytic Material for the Remediation of Pollutants in Industrial Wastewater: A Review. *Catalysts*. 2020; **10**(12): 1–54. DOI: https://doi.org/10.3390/catal10121435.

[18] Sharma D and Mehta BR. Nanostructured TiO_2 Thin Films Sensitized by CeO_2 as an Inexpensive Photoanode for Enhanced Photoactivity of Water Oxidation. *Journal of Alloys and Compounds*. 2018; **749**: 329–335. DOI: https://doi.org/10.1016/j.jallcom.2018.03.228.

[19] Lucid AK, Keating PRL, Allen JP, and Watson GW. Structure and Reducibility of CeO_2 Doped with Trivalent Cations. *Journal of Physical Chemistry C*. 2016; **120**(41): 23430–23440. DOI: https://doi.org/10.1021/acs.jpcc.6b08118.

[20] Murugadoss G, Ma J, Ning X, and Kumar MR. Selective Metal Ions Doped CeO_2 Nanoparticles for Excellent Photocatalytic Activity under Sun Light and Supercapacitor Application. *Inorganic Chemistry Communications*. 2019; **109**: 107577. DOI: https://doi.org/10.1016/j.inoche.2019.107577.

[21] Hebert SC and Stöwe K. Synthesis and Characterization of Bismuth-Cerium Oxides for the Catalytic Oxidation of Diesel Soot. *Materials*. 2020; **13**(6): 1369. DOI: https://doi.org/10.3390/ma13061369.

[22] Liu Y, et al. Bi-Doped Ceria with Increased Oxygen Vacancy for Enhanced CO_2 Photoreduction Performance. *Wuji Cailiao Xuebao/Journal of Inorganic Materials*. 2021; **36**(1): 88–94. DOI: https://doi.org/10.15541/jim20200142.

[23] Jiang D, et al. Bismuth-Induced Integration of Solar Energy Conversion with Synergistic Low-Temperature Catalysis in $Ce_{1-x}Bi_xO_{2-\delta}$ Nanorods. *Journal of Physical Chemistry C*. 2013; **117**(46): 24242–24249. DOI: https://doi.org/10.1021/jp4092943.

[24] Santra C, Auroux A, and Chowdhury B. Bi Doped CeO_2 Oxide Supported Gold Nanoparticle Catalysts for the Aerobic Oxidation of Alcohols. *RSC Advances*. 2016; **6**(51): 45330–45342. DOI: https://doi.org/10.1039/c6ra05216a.

[25] Efendi AF and Nurhasanah I. UV-Light Absorption and Photocatalytic Properties of Zn-Doped CeO_2 Nanopowders Prepared by Ultrasound Irradiation. *Materials Science Forum*, 2015; **827**: 56–61. DOI: https://doi.org/10.4028/www.scientific.net/MSF.827.56.

[26] Ansari AA and Kaushik A. Synthesis and Optical Properties of Nanostructured $Ce(OH)_4$. *Journal of Semiconductors*. 2010; **31**(3): 033001. DOI: https://doi.org/10.1088/1674-4926/31/3/033001.

[27] di Lauro C. *Rotational Structure in Molecular Infrared Spectra*. Netherlands: Elsevier; 2013. DOI: https://doi.org/10.1016/C2012-0-03393-5.

[28] Al-Otaibi AL, Howsawi E, and Ghrib T. Structural and Optical Characteristics of Pure and 5%RE (Tb, Y and Eu) Doped ZnO. *Nano-Structures and Nano-Objects*. 2020; **24**: 100551. DOI: https://doi.org/10.1016/j.nanoso.2020.100551.

[29] Ashraf R, Riaz S, Kayani ZN, and Naseem S. Effect of Calcination on Properties of ZnO Nanoparticles. *Material Today: Proceedings*, 2015; **2**(10B): 5468-5472. DOI: https://doi.org/10.1016/j.matpr.2015.11.071.

[30] Muche DNF, Souza FL, and Castro RHR. New Ultrasonic Assisted Co-Precipitation for High Surface Area Oxide Based Nanostructured Materials. *Reaction Chemistry and Engineering*. 2018; **3**(3): 244–250. DOI: https://doi.org/10.1039/c7re00183e.

[31] Gahrouei ZE, Imani M, Soltani M, and Shafyei A. Synthesis of Iron Oxide Nanoparticles for Hyperthermia Application: Effect of Ultrasonic Irradiation Assisted Co-Precipitation Route. *Advances in Natural Sciences: Nanoscience and Nanotechnology*. 2020; **11**(2): 025001. DOI: https://doi.org/10.1088/2043-6254/ab878f.